Tanzania Journal of Science 46(1): 61-75, 2020 ISSN 0856-1761, e-ISSN 2507-7961

Geochemical Characterization of the Paleoproterozoic Massif-Type Anorthosites from the Ubendian Belt, Tanzania

Nelson Boniface
University of Dar es Salaam, Geology Department, P. O. Box 35052, Dar es Salaam, Tanzania
E-mail address: nelson.boniface@udsm.ac.tz

Received 27 Oct 2019, Revised 27 Dec 2019, Accepted 1 Jan 2020, Published 31 Mar 2020

Abstract

Paleoproterozoic massif-type anorthosites occur in Southern Ubendian Belt (Upangwa Terrane) in Tanzania, mainly as mafic-plutons (meta-anorthosite and meta-gabbro) associated with ultramafic stocks and titaniferous magnetite bodies. Variably metamorphosed silicic granitoids are also recorded in the area. This article presents geochemical characteristics of meta-anorthosites, meta-gabbros and the associated granitoids in order to determine their genetic links and geotectonic settings. The meta-anorthosites, meta-gabbros and meta-tonalite have indistinguishable chondrite normalized REE patterns displaying LREE-enriched patterns (e.g., $(\mathrm{La/Sm})_N$ = 1.97–6.10) and negatively sloping HREE ($(\mathrm{La/Yb})_N$ = 4.05– 47.06) suggesting continental crustal affinity. The trace element patterns of the studied meta-anorthosites are characterized by enrichments of Eu and Sr, which is a typical signature of plagioclase dominated cumulates. The MORB-normalized trace element patterns of meta-anorthosites and meta-gabbros resemble the average continental arc trace element patterns. Likewise, trace element ratios (e.g., Th/Yb and Nb/Yb) Upangwa Terrane plutons point to their crystallization at a continental arc probably between 1920 and 1850 Ma.

Keywords: Ubendian Belt, Massif-type Anorthosites, Trace Element Geochemistry, Tanzania

Introduction

Proterozoic massif-type anorthosites commonly occur in ancient Andean-type continental arc setting with coeval, but not consanguineous, suite of silicic plutons (Torsvik 2003, Arndt 2013, Ashwal and Bybee 2017). Massif-type anorthosites are mantle-derived basaltic melts, which get arrested at the crustal-mantle boundary (Moho-depth) in continental arc environments, and the melts differentiate by crystallization of plagioclase cumulates leaving dense Fe-rich magma (Ashwal 1993, Arndt 2013, Ashwal and Bybee 2017).

The Ubendian Belt hosts massif-type anorthosites defined by the assemblage of mafic-ultra-mafic bodies (e.g., Nkenza ultramafic platinum bearing bodies), gabbros, iron-ore, and anorthositic plutons known as the Upangwa Meta-Anorthosite Complex (Figure 1, Harpum 1958, Haldemann 1961, Evans et al. 2012, Manya and Maboko 2016). Metamorphosed silicic batholiths and less deformed K-rich granitoids and tonalite batholith (e.g., the Ubena granitoids) occur together with the Upangwa massifs (Figure 1, Harpum 1958, Haldemann 1961, Evans et al. 2012, Manya and Maboko 2016). Geochemical signature and petrographic features of the lower part of the Nkenza ultramafic body point to remnants of the upper oceanic crust ophiolite, which has affinity to continental crust (Evans et al. 2012). The aim of this study was to establish geochemical data from gabbros and anorthosites of the Upangwa massifs and use the data to propose the paleotectonic environment in which the massifs formed. The Upangwa massifs anorthosites are potential hosts of titanium, iron and platinum

metals of which origin is not fully understood due to limited published or known geological data.

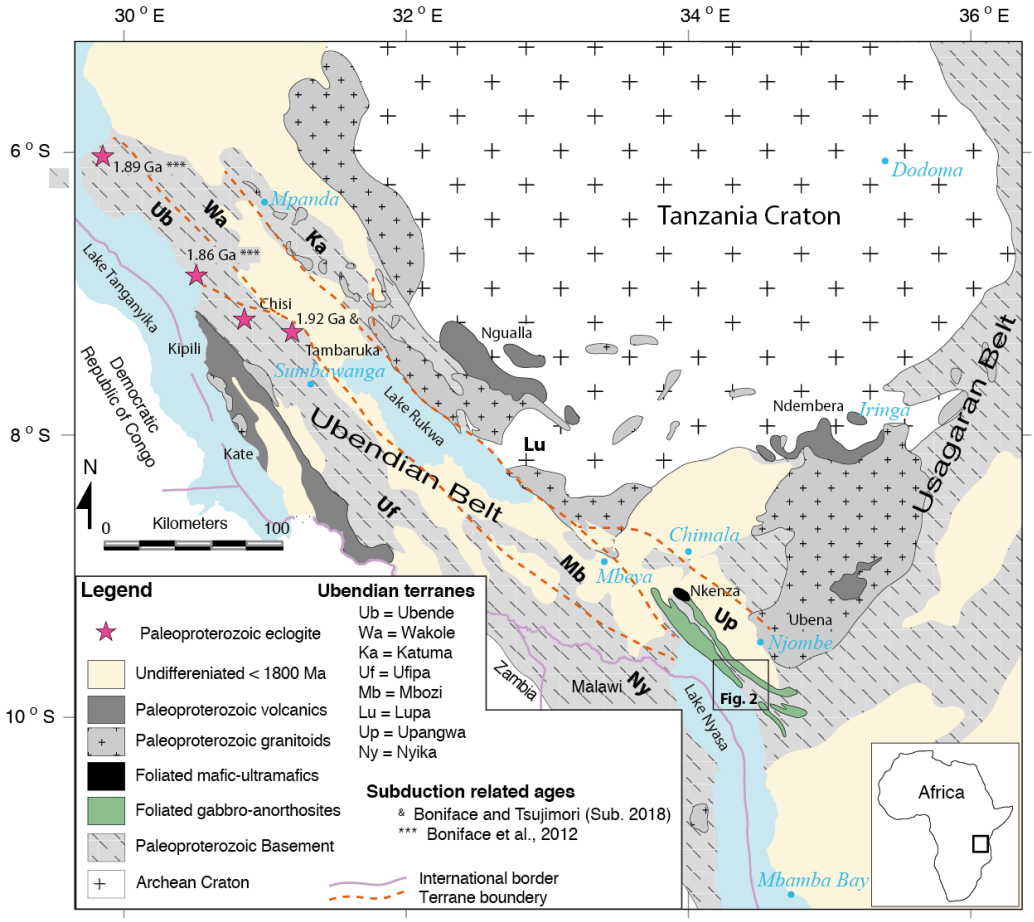

Figure 1: Geological map of the Upangwa terrane in southern Ubendian Belt. The Ubendian Belt terrane boundary is according to Daly (1988) and the map was modified after Pinna et al. (2004) and Legler et al. (2015).

Geological Background

The study area is located at the southern end of the Ubendian Orogenic Belt where is locally known as the Upangwa Terrane (Daly 1988). The Upangwa Terrane is one of the several lithotectonic terrains of the Ubendian Belt, which is mainly characterized by large masses of metamorphosed mafic igneous rock complex that range from meta-anorthositic to meta-gabbroic batholiths. The gabbroic and anorthositic batholiths intruded lower crustal rocks (para-gneisses: e.g., biotite gneisses, garnet–biotite–sillimanite gneisses: and orthogneisses: e.g., amphibolites, granulites and felsic gneisses) (Figure 2, Harpum 1958, Evans et al. 2012, Said and Kamihanda 2015, Boniface and Appel 2017).

The mafic-ultramafic igneous rocks of the Upangwa Meta-Anorthosite Complex range from non-foliated apparently non-metamorphic to highly metamorphosed rocks reaching up to amphibolite and granulite facies metamorphic conditions

with garnet and migmatite in places (Harpum 1958, Haldemann 1961). The paragneisses (garnet–biotite–sillimanite gneisses) in the Upangwa Terrane are migmatized and overprinted by three metamorphic and deformation episodes dated at 1808 ± 9 Ma, 944 ± 4 Ma and 565 ± 4 - 559 ± 8 Ma (Boniface and Appel 2017).

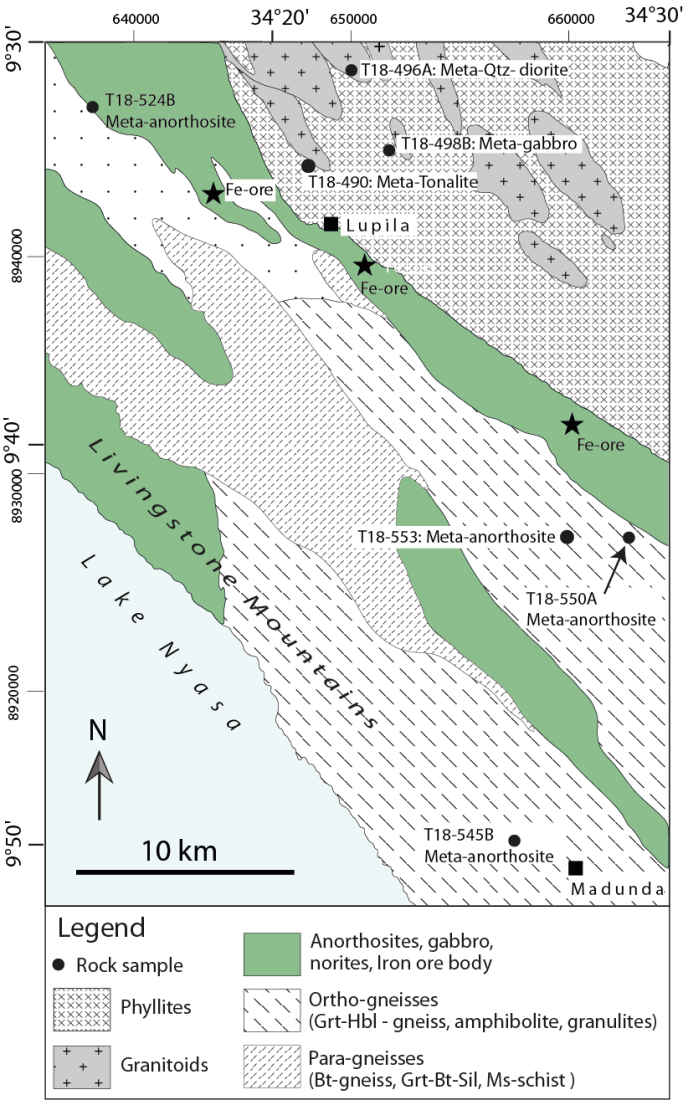

Figure 2: Geological map of the study area illustrating sample location sites and field lithological relations, modified from QDS 273 after Said and Kamihanda (2015).

The Ubendian orogenic cycle records a subduction event date between 1920 and 1860 Ma, which is coeval with emplacements of explosive volcanics (e.g., Ngualla and Ndembera volcanics) and pluton complexes (granitic intrusives and gabbro-anorthosite complexes) (Figure 1, Collins et al. 2004, Boniface et al. 2012, Bahame et al. 2016, Tulibonywa et al. 2015). Isotopic and geochemical characteristics of the volcano-

plutonic rocks in the Ubendian-Usagaran Belt point to their emplacement in volcanic arc settings that probably accompanied the Ubendian-Usagaran subduction cycles at the margins of the Tanzania Craton (see Lawley et al. 2013, Tulibonywa et al. 2015, Bahame et al. 2016, Manya and Maboko 2016).

The Ubendian Belt (Lupa Terrane) is intruded by Ngualla metavolcanics (meta-rhyolite, meta-dacite, meta-andesite, and meta-agglomerate), metabasites (diorite, appinite, and gabbro), and biotite ± hornblende-granites, hornblende-granodiorite, syenogranite, biotite-muscovite granite that were emplaced between 1959.6 ± 1.1 and 1919 ± 37 Ma (Figure 1, Lawley et al. 2013, Tulibonywa et al. 2015, Thomas et al. 2016). The entire package of pluto-volcanic rocks in the Lupa Terranes have strong calc-alkaline magmas affinity and have REE elements with features like magmas that erupt in the continental convergent margins (Lawley et al. 2013, Tulibonywa et al. 2017).

Likewise, along the Usagaran Belt, the calc-alkaline Ndembera metavolcanics with crystallization age between 1921 ± 14 and 1871 ± 15 Ma are coeval with foliated syntectonic granitoids and orthogneisses, which intruded along ductile strike-slip shear zones between 1942 ± 89 and 1877 ± 7 Ma probably in the continental arc setting (e.g., Sommer et al. 2005, Bahame et al. 2016, Thomas et al. 2019). Similar crystallization ages between 1887 ± 11 and 1857 ± 19 Ma are documented from high-K, I-type granites, and tonalites that crop out around Njombe town in southern Ubendian Belt (Figure 1, Manya and Maboko 2016). Generally, the granitoids and metavolcanics (Ndembera metavolcanics, syntectonic granitoids, and the late Usagaran granitoids) share similar geo-chemical features including very coherent REE patterns that are characterized by enrichment of the LREE relative to the HREE and depletion of HFSE (Nb-Ta, and Ti) which are a typical signatures for arc magmas (Bahame et al. 2016, Manya and Maboko 2016).

Materials and Methods

Rock samples

At outcrop scale, meta-anorthosites are foliated, variably deformed and clearly display layers of elongate crystals of mafic minerals (commonly clinopyroxene, ilmenite, magnetite and garnet) up to centimetre to millimetre scale (Figure 3a & b). Clinopyroxene, garnet, and magnetite concentrate in dark metamorphic bands (Figure 3b). Meta-gabbros are also foliated, however, the degree of foliation is not as strong as in anorthosites (Figure 3c). Rock units that are mainly composed of magnetite (magnetite ore) occur in association with gabbroic and anorthositic rock masses (Figure 3d).

Photomicrographs display clear deformation fabrics in meta-anorthosites, in which plagioclase porphyroclasts are stretched, kinked and their margins are partly recrystallized to fine-grained polygonal aggregates of untwinned grains of plagioclase (Figure 4a). Meta-gabbros mainly consist of undeformed clinopyroxene and plagioclase and minor amount of magnetite (Figure 4b).

Methods

Seven fresh rock samples (four meta-anorthosites, one meta-gabbro, and two silica rich rocks) were taken for petrographic examination and description and geochemical investigations. Sample locations, lithology types and coordinates are provided in Figure 2 and Table 1. The samples were crushed and milled by using an agate mill at the African Minerals and Geoscience Centre. Bulk-rock analyses of each powdered sample were carried out at Activation Laboratories Ltd., Canada, using Code 4Litho package. The package uses fusion inductively coupled plasma opticalemission spectrometry (FUS-ICPOES) and inductively coupled plasma mass spectroscopy (FUS-ICPMS) for the major and trace element analyses, respectively. Fused samples were diluted and analysed by Perkin

Elmer Sciex ELAN 6000, 6100 or 9000 ICP-MS. Three blanks and five control samples (three before sample group and two after) were analysed per group of samples. Details of sample preparation and analytical procedures for major and trace elements at the Activation commercial Laboratories are as described in the Litho-geochemistry Packages manual available online or by request (www.actlabs.com: +18882285227: fusion process 4B).

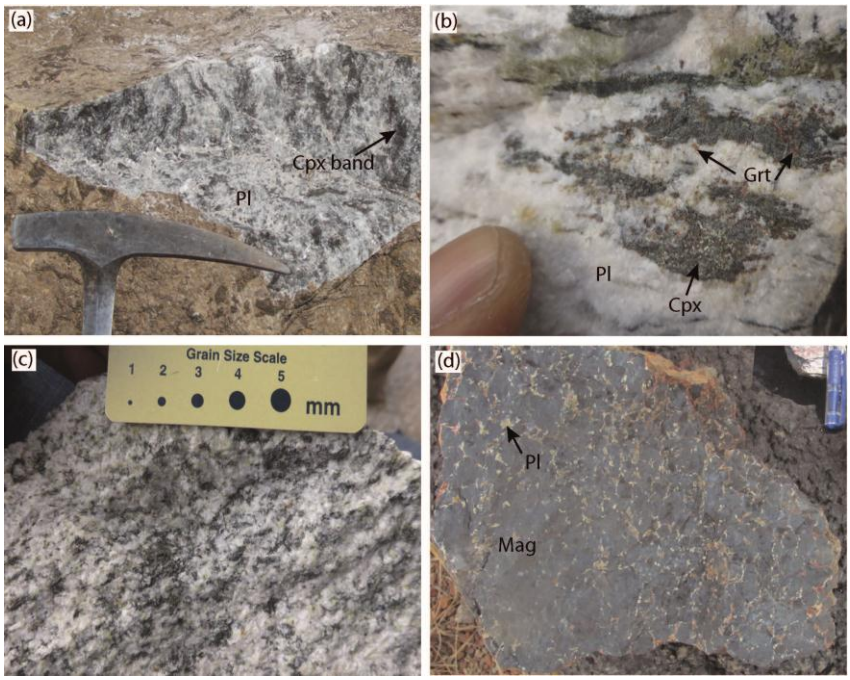

Figure 3: Sample images of meta-anorthosites, meta-gabbros and iron ore from southern Ubendian Belt. (a) Appearance of a banded anorthosite at the outcrop (b) Garnet in dark bands of meta-anorthosites. (c) Slightly foliated meta-gabbros. (d) Iron ore sample.

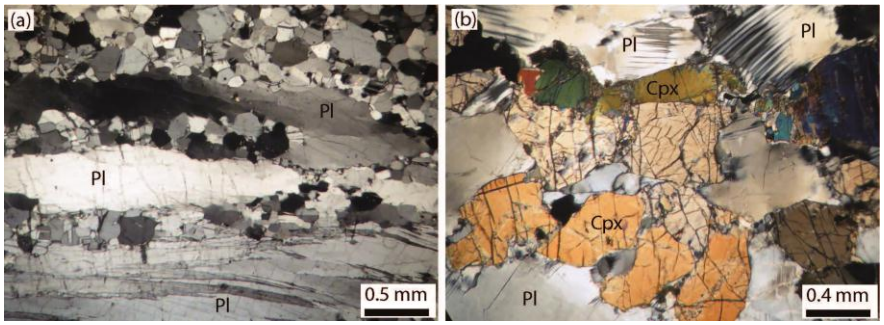

Figure 4: Thin section images (a) Mortared and kink banded and twinned plagioclase porphyroclasts surrounded by recrystallized granoblastic equivalents (the same mineral) in meta-anorthosites. (b) Slightly deformed clinopyroxene and plagioclase in gabbros.

Results

Data for the major and trace elements of the meta-anorthosites, meta-gabbro and other rocks (tonalite and a quartz-monzogabbro) from southern Ubendian Belt are presented in Table 1 and their geochemical features are described below.

Table 1: Compositions of major and trace elements of the meta-anorthosites, meta-gabbros and granitoids from southern Ubendian Belt

Sample	T18-490	T18-496A	T18-498B	T18-524B	T18-545B	T18-550A	T18-553
Lithology	Meta-Tonalite	Meta-Quartz-diorite	Meta-gabbro	Meta-anorthosite	Meta-anorthosite	Meta-anorthosite	Meta-anorthosite
UTM Coordinate	648281 8944534	650344 8949051	652363 8944781	638630 8946900	657964 8912976	663269 8926834	659606 8926951
Major elements (wt. %)							
SiO_2	66.11	71.25	50.07	53.01	49.59	50.71	51.3
TiO_2	0.293	0.184	0.848	0.145	0.992	0.234	0.451
Al_2O_3	15.69	13.43	26.99	26.99	25.51	22.91	26.84
FeO (t)	3.49	2.22	4.58	1.68	5.28	6.3	3.45
MnO	1.059	1.039	0.255	0.344	0.804	0.255	0.219
MgO	1	0.15	1.02	0.66	1.27	7.53	1.4
CaO	4.14	0.85	13.86	10.45	13.63	8.41	11.01
Na_2O	4.6	3.81	2.16	4.81	2.11	3.54	4.44
K_2O	1.24	4.92	0.34	0.48	0.4	0.24	0.44
P_2O_5	0.15	0.03	0.15	0.03	0.17	0.01	0.02
LOI	0.87	0.65	0.39	1.19	0.44	0.31	0.75
Total	98.65	98.53	100.7	99.77	100.2	100.5	100.3
Trace elements (ppm)							
Co	13	8	13	6	18	33	11
Cu	40	20	40	10	30	40	10
Ni	20	20	60	70	20	140	40
Mn	0	0	0	0	0	0	0
Zn	50	70	60	30	60	50	30
Cr	20	20	30	50	20	220	30
Sc	3	2	8	1	8	13	7
V	52	6	60	19	62	65	79
Mo	4	9	3	2	2	6	2
Cs	1.1	0.5	0.2	0.1	0.1	0.1	0.1
Rb	55	200	1	2	1	1	1
Ba	2926	2781	370	877	1963	404	602
Th	1.5	38.8	2.28	0.11	0.78	2.73	0.13
U	0.41	5.85	10.2	0.23	0.17	5.58	0.22
Nb	10.3	47.1	313	4.6	6.2	106	4.4
Ta	1.53	6.29	500	4.63	0.87	383	9.03
K	10293.86	40843.38	2822.51	3984.72	3320.6	1992.36	3652.66
La	12.6	89.2	12.6	3.49	11.2	2.43	2.7
Ce	19	141	25.9	6.5	23.5	4.12	5.47
Pb	13	28	23	7	5	7	5
Pr	2.21	15.5	2.99	0.63	2.66	0.51	0.73
Sr	721	90	469	726	446	500	673
P	0	0	0	0	0	0	0
Nd	8.38	51.3	12.2	2.12	10.4	2.01	3.4
Zr	131	264	34	3	33	13	10
Hf	3	8.6	2.9	0.1	0.8	2.2	0.3

Sample	T18-490	T18-496A	T18-498B	T18-524B	T18-545B	T18-550A	T18-553
Lithology	Meta-Tonalite	Meta-Quartz-diorite	Meta-gabbro	Meta-anorthosite	Meta-anorthosite	Meta-anorthosite	Meta-anorthosite
Sm	1.43	8.44	2.58	0.36	2.17	0.55	0.86
Eu	0.756	1.11	1.65	0.464	1.43	0.368	0.638
Ti	0.34	0.61	0.15	0.06	0.06	0.05	0.05
Gd	1.09	8.29	2.49	0.16	2.22	0.88	0.85
Tb	0.16	1.46	0.41	0.03	0.3	0.13	0.14
Dy	0.75	9.94	2.06	0.16	1.71	0.71	0.8
Y	4.5	92.7	10.8	0.7	9.1	5	4.6
Ho	0.14	2.29	0.35	0.02	0.33	0.13	0.17
Er	0.39	7.64	1	0.06	1	0.35	0.5
Tm	0.057	1.13	0.135	0.008	0.149	0.049	0.073
Yb	0.38	7.65	0.86	0.05	0.97	0.33	0.45
Lu	0.06	1.16	0.127	0.008	0.143	0.054	0.065
$K_2O + Na_2O$	5.84	8.73	2.50	5.29	2.51	3.78	4.88
Mg#	33.81	10.75	28.42	41.19	30.01	68.06	41.98
Eu/Eu*	0.41	1.85	1.99	5.91	1.99	1.62	2.28
$(La/Sm)_N$	6.65	5.54	3.07	6.10	3.25	2.78	1.97
$(La/Yb)_N$	7.86	22.35	9.88	47.06	7.78	4.96	4.05
$(Gd/Yb)_N$	0.87	2.31	2.34	2.58	1.85	2.15	1.52
Th/Yb	5.07	3.95	2.65	2.20	0.80	8.27	0.29
Nb/Yb	6.16	27.11	363.95	92.00	6.39	321.21	9.78
Ta/Yb	7.49	6.73	0.63	0.99	7.13	0.28	0.49
Normative mineralogy (wt. %)							
Plagioclase	57.42	36.26	81.22	91.34	76.81	71.61	88.94
Orthoclase	7.33	29.08	2.01	2.84	2.36	1.42	2.60
Quartz	24.90	28.30	6.45	0.12	6.80	0.00	0.00
Magnetite	2.62	2.87	0.00	0.68	0.00	0.18	0.00
Hypersthene	2.11	0.37	1.50	1.28	0.55	18.70	0.00
Hematite	1.68	0.24	4.58	1.21	5.28	6.17	3.45
Ilmenite	0.55	0.34	0.56	0.28	1.71	0.44	0.47
Diopside	0.82	0.00	2.25	0.79	5.64	0.00	1.39

Note: LOI = Loss of volatiles on ignition

The normative mineral compositions for plagioclase in the range between 91.34 and 71.61 wt. % indicate the abundance of plagioclase over other minerals in meta-anorthosites and meta-gabbros (Table 1). The presence of significant amount of ilmenite (1.71–0.28 wt. %) reflects the saturation of TiO_2 in these rocks. Meta-tonalitic and meta-quartz-dioritic samples have significant amounts of normative quartz as suggested in petrographic analysis (Table 1).

Meta-anorthosites and meta-gabbros

Meta-anorthosites and meta-gabbros are compositionally uniform having major elements at 49.59–53.01 wt.% SiO_2, 22.91–26.99 wt.% Al_2O_3, 0.15–0.99 wt.% TiO_2, and 2.50–5.29 wt.% ($K_2O + Na_2O$). The composition of fluid mobile elements range at 0.1–0.2 ppm Cs, and 1–2 ppm Rb: and fluid immobile elements at 0.05–0.15 ppm Ti, 0.1–2.9 ppm Zr, 0.1–2.9 ppm Hf. However, they possess moderately variable MgO (0.66–7.53 wt.%), Mg# (28.42–68.06), Co (6–33 ppm), Ni (20–140 ppm), and Cr (20–220 ppm), V (19–79 ppm), Sc (1–13 ppm), and Zr (3–34 ppm) abundances. The abundances of REE elements are uniform to moderately variable (Table 1). Large variations are observed in Ba (370–1963 ppm), Sr (446–

726 ppm), Nb (4.4–313 ppm), and Ta (0.87–500 ppm).

Meta-anorthosites and meta-gabbros are sub-alkaline with basaltic to andesitic composition (SiO_2 = 49.59–53.01 wt.%) (Figure 5a). However, it should be noted that alkali vs sub-alkali diagrams are aimed to distinguish for melt products rather than cumulus rocks. Major elements, e.g., (K_2O + Na_2O) and (FeO + MnO + MgO + TiO_2) show correlations with SiO_2 (Figure 5b). Likewise, variation diagrams of selected fluid mobile and fluid immobile elements, e.g., Sr, Ba, Nb, Gd, Sm, Hf, and TiO_2 display strong correlations with Zr (Figure 5c - i). On a chondrite-normalized Rare Earth Element (REE) diagram, meta-anorthosites, meta-gabbros have indistinguishable patterns with remarkably positive Eu anomaly. The REE patterns display a uniform negative slope with enrichment of LREE over MREE (La_N /Sm_N: 1.97–6.10) and HREE (La_N /Yb_N : 4.05–47.06), and (Gd_N /Yb_N: 1.52–2.58) (Figure 6a). The chondrite-normalized La values range between 8 and 288 times chondritic values and the chondrite normalized La/Lu ratios vary from 4.3 to 45.3. On a MORB-normalized trace element diagram, strong spikes of Eu, Sr, Pb, Ta, and Ba characterize all the samples. However, the diagram shows negative anomalies of Rb, Th, Nb, La, Ce, Pr, Zr and Hf. With the exception of the presence of Eu spike and lack of Ta trough, the general patterns of the meta-anorthosites and meta-gabbro resemble the average continental arc trace element patterns (Figure 6c, Kelemen et al. 2003).

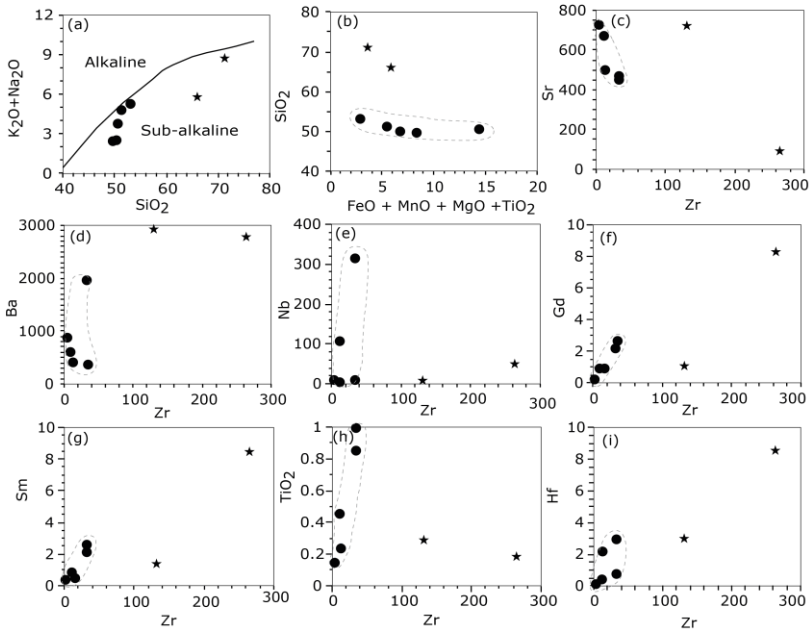

Figure 5: Variation diagrams of the studied rocks samples. Black filled dots represent meta-anorthosites and meta-gabbros composition and the asterisks are for a meta-tonalite and meta-quartz-diorite. (a) (K_2O + Na_2O) against SiO_2. (b) SiO_2 against (FeO + MnO + MgO + TiO_2). (c) to (i) Zr vs. selected element variation diagrams to highlight the correlations among the fluid mobile and fluid immobile elements.

Tanzania Journal of Science 46(1): 61-75, 2020 ISSN 0856-1761, e-ISSN 2507-7961

Meta-tonalite and meta-quartz-diorite

One sample each for a meta-tonalite and a meta-quartz-diorite lithologies are briefly described below and their compositions are presented in Table 1. Both rock samples, tonalite with SiO_2 = 66.11 wt.% and quartz-monzogabbro SiO_2 = 71.25 wt.% are silica richer but lower CaO (0.85 - 4.14 wt.%) contents than the anorthosites. In all variation diagrams for major elements and trace elements, the tonalite and quartz-diorite do not follow differentiation trends displayed by anorthosites.

On a chondrite-normalized trace element diagram, the meta-tonalite display similar pattern like that observed in meta-anorthosites (e.g., negative slope with enrichment of LREE over MREE and positive Eu anomaly) (Figure 6a and b). Likewise, the meta-diorites display a negative slope with enrichment of LREE over MREE but negative Eu anomaly (Figure 6a and b). On a MORB-normalized trace element diagram, both the meta-tonalite and meta-quartz-diorite show patterns that are similar to what is displayed by meta-anorthosites and meta-gabbros (e.g., spikes on Eu, Sr, Pb, Ta, and Ba and negative anomalies of Rb, Th, Nb, La, Ce, Pr, Zr and Hf) except the negative Eu and Sr anomalies on a meta-quartz-diorite (Figure 6d).

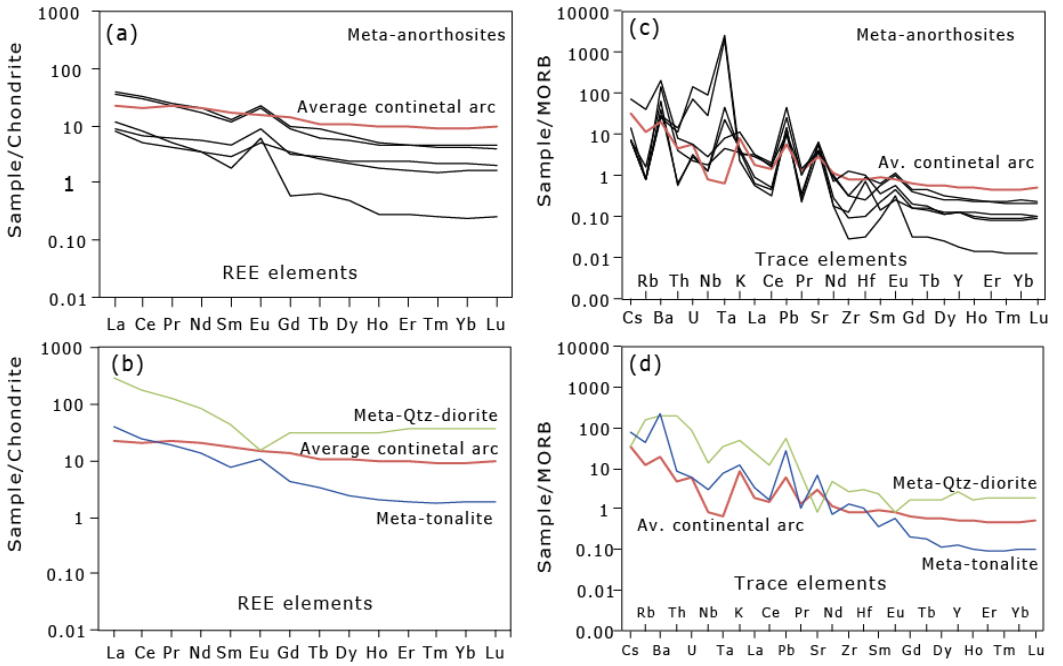

Figure 6: (a and b) Chondrite - normalized rare earth element spidergrams highlighting the REE patterns of the Upangwa meta-anorthosites and other rock types, the normalizing data are from (Boynton 1984) and the average arc is from (Kelemen et al. 2003). (c and d) MORB - normalized trace element spidergrams, the normalizing data are from (Hofmann 1988).

Discussion

The boundaries of coarse-grained plagioclase crystals in anorthosites are mortared and recrystallized to granoblastic equivalents of the same mineral. The isolated crystals of magnetite, ilmenite, and clinopyroxene display a preferred orientation. Dark layers in meta-anorthosites have disseminated garnets indicating metamorphic overprints possibly at amphibolite facies conditions. Effects of deformation and metamorphism on element mobility in the Upangwa Terrane meta-anorthosites and meta-gabbros were evaluated by using variation diagrams (Figure 5a-h). The meta-anorthosites and meta-gabbros are compositionally uniform and have moderately variable major elements, fluid mobile elements and fluid immobile elements. Moreover, the variation diagrams for major elements, fluid mobile elements and fluid immobile elements display strong correlations, which indicate that these elements were not significantly disturbed by post-magmatic tectonic events (Polat and Hofmann 2003). Hence this observation indicates that petrogenesis and tectonic settings of the metamorphosed Upangwa Terrane meta-anorthosites and meta-gabbros are determined by evaluating the geochemical signatures of the major elements, fluid mobile elements, and fluid immobile elements.

The SiO_2 contents in meta-anorthosites and meta-gabbros range from 49.59 to 53.01 wt.% showing a basaltic to intermediate composition. The meta-quartz diorites (SiO_2 = 71.25 wt.%) and meta-tonalite (SiO_2 = 66.11 wt.%) are more evolved to granitic composition. The composition of Al_2O_3 between 22.91 and 26.99 wt.% indicate that the sampled Upangwa Terrane meta-anorthosites and meta-gabbros belong to high-alumina group. Rocks that contain Al_2O_3 > 20 wt.% are considered to as cumulates (Pearce 1996), and the high alumina content in meta-anorthosite is contributed by the abundance of plagioclase. Therefore, high amounts of Al_2O_3, (22.91–26.99 wt%) CaO (8.41–13.86 wt.%) and Na_2O (2.11–4.81 wt.%) reflect high amounts of cumulus plagioclase. When using basalts discrimination to such kind of rocks, the chemical effects of crystal accumulation should be taken into account (Pearce 1996).

The Upangwa Terrane meta-anorthosites, meta-gabbros and the associated meta-tonalite have indistinguishable chondrite normalized REE patterns (Figure 6a&c). All the sampled rock types have light REE-enriched patterns (e.g., $(La/Sm)_N$ = 1.97 - 6.10) and negatively sloping heavy REE ($(La/Yb)_N$ = 4.05 - 47.06) indicating the continental crustal affinity (Pearce and Cann 1973, Pearce 1996). Generally the observed trace patterns on the chondrite normalized diagram (Figure 6a) and MORB normalized diagram (Figure 6b) show similarities to the patterns of the average arc (Kelemen et al. 2003). On an N-MORB-normalized trace element diagram (Figure 6b), the samples display elevated concentrations of slab-derived components (Cs, Rb, Ba, U, K, La, Ce, Pb, Sr) that are superimposed on conservative mantle wedge derived components (Nb, Zr, Sm, Eu, Dy, Y, Yb, Lu), therefore producing the distinctive pattern of spikes and troughs. The strong positive Eu anomaly is a common signature in anorthosites due to its substitution and enrichment in plagioclase cumulates (Arndt 2013, Ashwal and Bybee 2017). A high Ta content observed in meta-anorthosites is associated with the saturation TiO_2 and eventually crystallization of ilmenite because Ta and other trace elements are compatible in oxide structures (Seifert et al. 2010).

The presentation of the Upangwa Terrane anorthosites and associated rocks on the MORB normalized trace element diagram of Pearce (1983) on Figure 7, indicates that granitoids (meta-quartz diorite and meta-tonalite, Figure 7a) have trace element patterns similar to the continental arc magmas, which are characterized by selective

enrichments of low ionic potential elements or fluid mobile elements (Sr, K, Rb, Ba, and Th) and low abundances of elements of high ionic potential or fluid immobile elements (Ta, Nb, Ce, Zr, Hf, Sm, Y, and Yb) compared to N-type MORB. The enrichment of low ionic potential elements is attributed to metasomatism of the mantle source of arc basalts by fluids released from the subducted slabs (e.g., Pearce 1983). Similar trace elements patterns are displayed by the nearby Ubena high-K, I-type granites, and tonalites (emplaced between 1887 ± 11–1820 ± 9 Ma) and the Nkenja mafic-ultramafic rocks (Figure 7b & c, data from Manya and Maboko 2016, Evans et al. 2012).

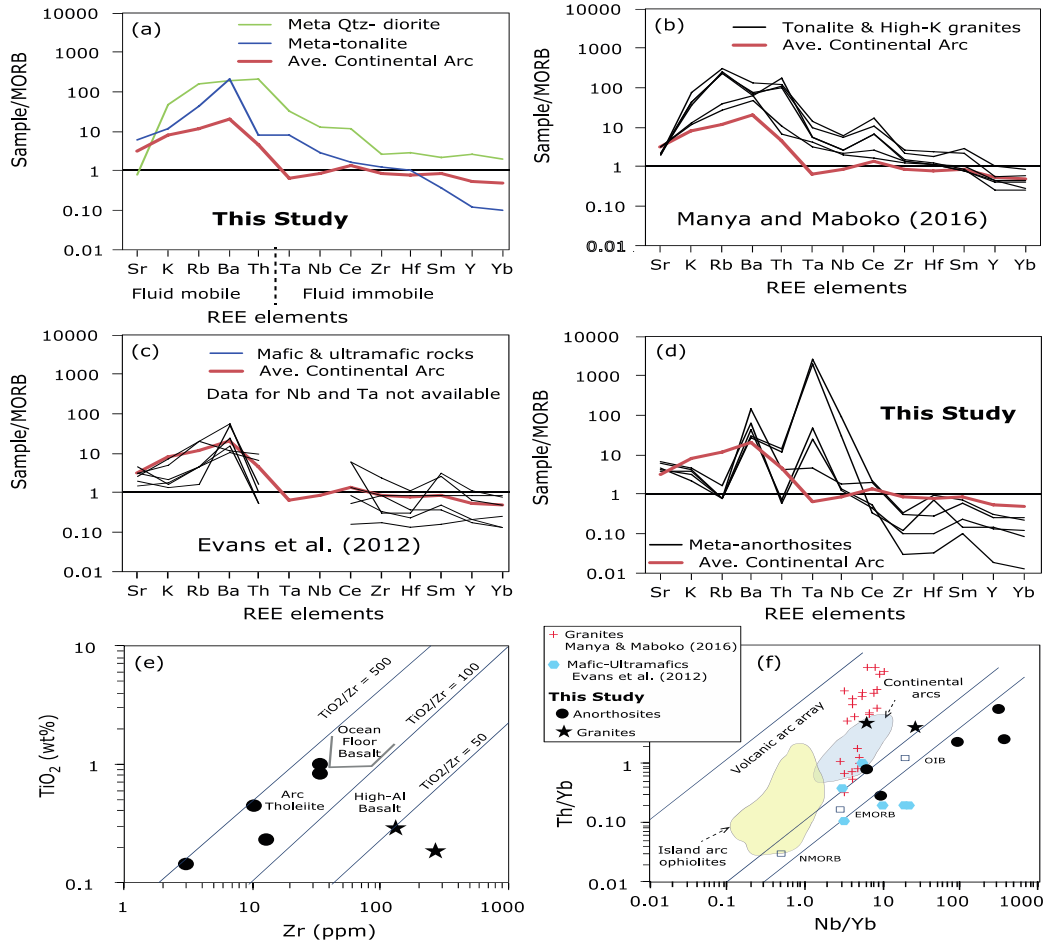

Figure 7: (a to d) MORB normalized trace element diagram, after Pearce (1983), comparing data from the Upangwa Terrane and magmas from active continental margins, (active continental margins data from Kelemen et al. (2003)) (a) data for meta-quartz diorite and meta-tonalite from this study (b) data for tonalites and high-K granites from Manya and Maboko (2016) (c) data for meta-anorthosites and meta-gabbro from this study (d) data for mafic and ultramafic rocks from Evans et al. (2012) (e) TiO_2 against Zr variation diagram (fields are from Dietrich et al. (1981) (f) Th/Yb against Nb/Yb diagram after Pearce (1983) and island arc ophiolites data from Mohan et al. (2013).

On the MORB normalized trace element diagram (Figure 7d), the meta-anorthosites and meta-gabbro have patterns of fluid immobile elements (i.e., Zr, Hf, Sm, Y and Yb) similar to that of the Nkenza mafic-ultramafic rocks (Figure 7c). However, the trace element patterns of meta-anorthosites and meta-gabbro deviate from continental arc magmas by having notable enrichments on Nb and Ta, and depletions on Rb and Th. On the TiO_2 and Zr (Figure 7e) the meta-anorthosites and meta-gabbro resemble arc tholeiites. Enrichment in some trace elements (Figure 7) is attributed to the abundance of particular mineral species, e.g., plagioclase (Ba), ilmenite (Ta, Nb) possibly resulting from cumulate process (Gleißner et al. 2011). The depletion of Th is probably related to crystal-magma segregation processes that might have reduced the abundance of Th bearing minerals.

Trace element ratios (Th/Yb and Nb/Yb) of the Upangwa Terrane anorthosite massifs and the associated granitoids are completely matching the compositions of continental arc magmas (Figure 7f). Some meta-anorthosites and meta-gabbros have compositional range similar to the mafic-ultramafic rocks from the nearby unit of the Nkenza mafic-ultramafic body (Figure 7d&f, Evans et al. 2012). The meta-tonalites and meta-quartz diorite have elevated Th values, therefore plotting in the field of continental arc basalts together with data of tonalites and high-K granites from Manya and Maboko (2016). The tonalites and high-K granites from Manya and Maboko (2016) display a continuous elevation of the Th from the mantle array to the volcanic arc array (continental arc) (Figure 7f).

The data from this study indicate that the meta-anorthosites and meta-gabbros were derived from the same magma sources as the Nkenza mafic-ultramafic rocks, which show affinity to upper oceanic crust (a dismembered ophiolite) and continental crust (e.g., Evans et al. 2012). Therefore, the Upangwa massif-type anorthosites, mafic-ultramafic rocks, and the associated granitoids (tonalites, diorites, and high-K granites) were formed at the active continental margins in southern Ubendian Belt.

Granitoids and calc-alkaline volcanics in southern Ubendian Belt were formed at active continental margins and have crystallization ages between 1927 ± 7 and 1857 ± 19 Ma (see Manya and Maboko 2016, Thomas et al. 2019), which is probably the emplacement age range for the Upangwa massif-type anorthosites. The onset of active continental margins recorded in tonalites and high-K granites and calc-alkaline volcanics is coeval with the onset of subduction of oceanic lithosphere along the Ubendian Belt between 1890 Ma and 1860 Ma (Boniface et al. 2012). Another unit of mineralized (corundum-bearing, i.e., ruby and sapphire) meta-cumulate rocks also occur at the subducting settings of the 2.0 Ga Usagaran Belt (Mori et al. 2019). Which implies that the Paleoproterozoic cumulates in the Ubendian-Usagaran Belt are potential sites for metallic and gemstone deposits.

Conclusions

The massif-type anorthosites of the Upangwa Meta-Anorthosite Complex in southern Ubendian Belt are mainly composed of deformed and metamorphosed anorthosites and gabbros, which intruded a high-grade Paleoproterozoic metamorphic basement. Geochemical characteristics of the rock assemblages (mafic-ultramafic bodies and the associated silicic granitoids) of the Upangwa Meta–Anorthosite Complex (e.g., Th/Yb and Nb/Yb ratios and REE patterns) point to their crystallization at active continental margins. The Upangwa Meta-Anorthosite Complex occurs together with variably deformed and metamorphosed syntectonic silicic granitoids (tonalites, diorites, high-K granites, and

granodiorites) with affinity to magmas that form at active continental margins. The crystallization age of the granitoids is known to be between 1927 ± 7 – 1857 ± 19 Ma (Manya and Maboko 2016, Thomas et al. 2019), which is concomitant with the ages of arc related metavolcanics at Ngualla (in the Ubendian Belt) and Ndembera (in the Usagaran Belt) (Tulibonywa et al. 2015, Bahame et al. 2016). The crystallization ages of the granitoid and metavolcanics in the Ubendian and Usagaran Belt are coeval with the episodes of subduction events dated between 1890–1860 in the Ubendian Belt (Boniface et al. 2012, Tulibonywa et al. 2015, Bahame et al. 2016, Manya and Maboko 2016, Thomas et al. 2019). Therefore, the Massif-type anorthosites in southern Ubendian Belt were probably emplaced at active continental margins following the 1890–1860 Ma subduction events and the emplacement of calc-alkaline magmas and syntectonic silicic granitoids along the Tanzania Craton.

Acknowledgements

I acknowledge the support of the Geological Survey of Tanzania for thin section preparation and logistical support. I highly appreciate the Tanz. J. Sci. Chief Editor Prof. John A. M. Mahugija, and the anonymous reviewers for handling the manuscript with enthusiasms. Specific persons who assisted my research at different stages include Abdul Mruma, Msechu Maruvuko, Khalid Musa Nyoka, Godson Kamihanda and Hamisi Saidi. Costs for analysing samples were met privately by the author.

References

Arndt N 2013 The formation of massif anorthosite: Petrology in reverse. *Geoscience Front.* 4: 195-198.

Ashwal LD 1993 Anorthosites. *Springer-Verlag Berlin* pp 422.

Ashwal LD and Bybee GM 2017 Crustal evolution and temporality of anorthosites. *Earth-Sci. Rev.* 173: 307-330.

Bahame G, Manya S and Maboko MA 2016 Age and geochemistry of coeval felsic volcanism and plutonism in the Palaeoproterozoic Ndembera Group of southwestern Tanzania: Constraints from SHRIMP U–Pb zircon and Sm–Nd data. *Precambrian Res.* 272: 115-132.

Boniface N and Appel P 2017 Stenian-Tonian and Ediacaran metamorphic imprints in the southern Paleoproterozoic Ubendian Belt Tanzania: Constraints from in situ monazite ages. *J. Afr. Earth Sci.* 133: 25-35.

Boniface N, Schenk V and Appel P 2012 Paleoproterozoic eclogites of MORB-type chemistry and three Proterozoic orogenic cycles in the Ubendian belt (Tanzania): Evidence from monazite and zircon geochronology and geochemistry. *Precambr. Res.* 192-195: 16-33.

Boynton WV 1984 Cosmochemistry of the rare earth elements: meteorite studies. In: Henderson P (Ed) Developments in Geochemistry (Vol. 2, pp. 63-114), Elsevier, Amsterdam.

Collins AS, Reddy SM, Buchan C and Mruma A 2004 Temporal constraints on Palaeoproterozoic eclogite formation and exhumation (Usagaran Orogen Tanzania). *Earth Planet. Sci. Lett.* 224 (1-2): 175-192.

Daly MC 1988 Crustal shear zones in Central Africa: a kinematic approach to Proterozoic tectonics. *Episodes* 11 (1): 5-11.

Dietrich VJ, Ganser A, Sommerauer J and Cameron WE 1981 Palaeogene komatiites from Gorgona Island East Pacific–A primary magma for ocean floor basalts. *Geochem. J.* 15: 141-161.

Evans DM, Barrett FM, Prichard HM and Fisher PC 2012 Platinum-palladium-gold mineralization in the Nkenja mafic-ultramafic body Ubendian metamorphic belt Tanzania. *Miner. Deposita* 47: 175-196.

Gleißner P, Druppel K and Romer RL 2011

The role of crustal contamination in massif-type anorthosites new evidence from Sr-Nd-Pb isotopic composition of the Kunene Intrusive Complex NW Namibia. *Precambr. Res.* 185 (1): 18-36.

Haldemann EG 1961 Geological Map, of Milo: Quarter degree sheet 274. Geological Map, *Geol. Survey Dept., Dodoma*.

Harpum JR 1958 Kipengere Quarter Degree Sheet 260 with brief explanation: 1: 125000 Map. Geological Map, *Geol. Survey Dept., Dodoma*.

Hofmann AW 1988 Chemical differentiation of the Earth: the relationship between mantle continental crust and oceanic crust. *Earth Planet. Sci. Lett.* 90 (3): 297-314.

Kelemen PB, Hanghøj K and Greene AR 2003 One view of the geochemistry of subduction-related magmatic arcs with emphasis on primitive andesite and lower crust. In: Rudnick R (Ed) The Crust Vol. 3, Treatise on Geochemistry (eds. HD Holland and KK Turekian) *Elsevier-Pergamon Oxford* pp. 593-659.

Lawley CJ, Selby D, Condon DJ, Horstwood M, Millar I, Crowley Q and Imber J 2013 Lithogeochemistry geochronology and geodynamic setting of the Lupa Terrane Tanzania: Implications for the extent of the Archean Tanzanian Craton. *Precambr. Res.* 231: 174-193.

Legler C, Barth A, Knobloch A, Mruma AH, Myumbilwa Y, Magigita M, Msechu M, Ngole T, Stanek KP, Boniface N, Kagya M, Manya S, Berndt T, Stahl M, Gebremichael M, Dickmayer E, Repper C, Falk D and Stephan T 2015 Minerogenic Map of Tanzania and Explanatory Notes for the Minerogenic Map of Tanzania 1:1.5 M. *Geol. Survey of Tanzania*.

Manya S and Maboko MA 2016 Generation of Palaeoproterozoic tonalites and associated high-K granites in southwestern Tanzania by partial melting of underplated mafic crust in an intracontinental setting: Constraints from geochemical and isotopic data. *Lithos* 260: 120-133.

Mohan MR, Satyanarayanan M, Santosh M, Sylvester PJ, Tubrett M and Lam R 2013 Neoarchean suprasubduction zone arc magmatism in southern India: geochemistry zircon U–Pb geochronology and Hf isotopes of the Sittampundi Anorthosite Complex. *Gondwana Res.* 23: 539-557.

Mori K, Tsujimori T and Boniface N 2018 Finding of talc-and kyanite-bearing amphibolite from the Paleoproterozoic Usagaran belt, Tanzania. *J. Miner. Petrol. Sci.* 113: 316-321.

Pearce JA 1983 The role of sub-continental lithosphere in magma genesis at destructive plate margins. In: Hawkesworth CJ, Norry MJ (Eds) Continental basalts and mantle xenoliths. *Shiva, Natwich* pp. 230-249.

Pearce JA 1996 A user's guide to basalt discrimination diagrams. In: DA Wyman (ed) Trace element geochemistry of volcanic rocks: applications for massive sulphide exploration *Geological Association of Canada*, Short Course Notes 12, pp. 79-113.

Pearce JA and Cann JR 1973 Tectonic setting of basic volcanic rocks determined using trace element analyses. *Earth and Planetary Science Letters* 19 (2): 290-300.

Pinna P, Muhongo S, Mcharo BA, Le Goff E, Deschamps Y, Ralay F and Milesi JP 2004 Geology and mineral map of Tanzania at 1: 2000000. *GST and BRGM*.

Polat A and Hofmann AW 2003 Alteration and geochemical patterns in the 3.7-3.8 Ga Isua greenstone belt West Greenland. *Precambrian Res.* 126: 197-218.

Said H and Kamihanda G 2015 Explanatory notes of the geology of Lupila: QDS 273-geology. Explanatory notes. *Geol. Survey of Tanzania*.

Seifert KE, Dymek RF, Whitney PR and Haskin LA 2010 Geochemistry of massif anorthosite and associated rocks, Adirondack Mountains, New York. *Geosphere* 6 (6): 855-899.

Sommer H, Kröner A, Muhongo S and

Hauzenberger C 2005 SHRIMP zircon ages for post-Usagaran granitoid and rhyolitic rocks from the Palaeoproterozoic terrain of southwestern Tanzania. *S. Afr. J. Geol.* 108: 247-256.

Thomas RJ, Jacobs J, Elburg MA, Mruma A, Kamihanda G, Kankila A, Masanja A and Saidi H 2019 New U-Pb-Hf zircon isotope data for the Paleoproterozoic Ubendian belt in the Chimala area SW Tanzania. *Geosci. Front.* 10(6): 1993-2006.

Thomas RJ, Spencer C, Bushi AM, Baglow N, Boniface N, de Kock G, Horstwood MS, Hollick L, Jacobs J, Kajara S, Kamihanda G, Key RM, Maganga Z, Mbawala F, McCourt W, Momburi P, Moses F, Mruma A, Myambilwa Y, Roberts NM, Saidi H, Nyanda P, Nyoka K and Millar I 2016 Geochronology of the central Tanzania Craton and its southern and eastern orogenic margins. *Precambr' Res.* 277: 47-67.

Torsvik TH 2003 The Rodinia jigsaw puzzle. *Science* 300: 1379-1381.

Tulibonywa T, Manya S and Maboko MA 2015 Palaeoproterozoic volcanism and granitic magmatism in the Ngualla area of the Ubendian Belt SW Tanzania: Constraints from SHRIMP U–Pb zircon ages and Sm–Nd isotope systematics. *Precambr. Res.* 256: 120-130.

Tulibonywa T, Manya S, Torssander P and Maboko MA 2017 Geochemistry of the Palaeoproterozoic volcanic and associated potassic granitic rocks of the Ngualla area of the Ubendian Belt SW Tanzania. *J. Afr. Earth Sci.* 129: 291-306.